75%-efficiency blue generation from an intracavity PPKTP frequency doubler

Rodolphe Le Targat, Jean-Jacques Zondy, Pierre Lemonde

HAL Id: hal-00002488
https://hal.science/hal-00002488

75%-efficiency blue generation from an intracavity PPKTP frequency doubler

R. Le Targat, J.-J. Zondy, P. Lemonde

BNM-SYRTE, Observatoire de Paris
61, avenue de l'observatoire, 75014 Paris, France

Abstract

We report on a high-efficiency 461 nm blue light conversion from an external cavity-enhanced second-harmonic generation of a 922 nm diode laser with a quasi-phase-matched KTP crystal (PPKTP). By choosing a long crystal ($L_C = 20$ mm) and twice looser focusing ($w_0 = 43\,\mu$m) than the "optimal" one, thermal lensing effects due to the blue power absorption are minimized while still maintaining near-optimal conversion efficiency. A stable blue power of 234 mW with a net conversion efficiency of $\eta = 75\%$ at an input mode-matched power of 310 mW is obtained. The intra-cavity measurements of the conversion efficiency and temperature tuning bandwidth yield an accurate value $d_{33}(461\,\text{nm}) = 15\,(\pm 5\%)$ pm/V for KTP and provide a stringent validation of some recently published linear and thermo-optic dispersion data of KTP.

Key words: Second harmonic generation, PPKTP, strontium, thermal effects
PACS: 42.65.Ky, 42.79.Nv, 42.70.Mp

1 Introduction

Continuous-wave (CW) high-power blue light generation is a key issue for many applications such as laser printing, RGB color display or for spectroscopy and cooling of atomic species. Due to the limited power and tunability of gas lasers (Ar$^+$, HeCd) or newly developed blue diode laser sources in the blue-UV spectrum [1], the usual procedure is to upconvert near-IR solid-state or semiconductor diode lasers either internal to the laser resonator [2] or in external enhancement resonators [3,4]. In the latter scheme, the efficiency of the upconversion is usually measured in terms of the ratio $\eta = P_{2\omega}/P_\omega^{\text{in}}$ of the generated second-harmonic (SH) power to the fundamental field (FF) power which is mode-matched to the resonator. Several nonlinear materials can upconvert

such lasers, using either temperature-tuned or angular birefringence phase-matching. The most widely used one is the large nonlinearity ($d_{\mathrm{eff}} \sim 18\,\mathrm{pm/V}$) potassium niobate (KNbO$_3$) crystal [5,6,7,8,9]. For temperature-tuned non-critical phase-matching, the major drawback of KNbO$_3$ is the occurrence of a phase transition leading to repoling near $T = 185°C$ [5,6], which restricts upconversion to laser wavelengths longer than $\lambda \sim 920\,\mathrm{nm}$. For laser cooling of the $^1S_0 - ^1P_1$ strontium line at 461 nm, which is the target of the present work, the use of a non-critically phase-matched KNbO$_3$ at $T \sim 150°C$ is hence not recommended. For shorter FF wavelengths, critical phase-matching at room-temperature is possible but results in a deleterious beam walk-off ($\rho \sim 1°$) of the blue wave – leading to elliptical beam shape or even higher-order transverse patterns [9] – combined with a narrow temperature band-width ($\Delta T \sim 0.5°C$) [8]. As an additional drawback, KNbO$_3$ is subject to blue-induced photo-chromic damage known as BLIIRA (Blue-Induced Infrared Absorption [10]). This nonlinear loss mechanism, together with the associated thermal lensing, has limited the highest reported conversion efficiency to $\eta \sim 80\%$, yielding 500 mW of blue power at 473 nm from a Nd:YAG laser power $P_\omega^{\mathrm{in}} \sim 800\,\mathrm{mW}$ [8].

Alternative widely used materials are LiB$_3$O$_5$ (LBO) or β-BaB$_2$O$_4$ (BBO) [11,12,13] but the low nonlinear coefficients of oxoborate crystals ($d_{\mathrm{eff}} \leq 1\,\mathrm{pm/V}$) are not suited to the frequency conversion of low power sources because it requires a tight control of the round-trip intracavity loss down to $\leq 1\%$. Recently, we employed a critically phase-matched KTP in a doubly-resonant sum-frequency generation (SFG) of a Nd:YAG laser and a low-power AlGaAs diode laser at 813 nm to produce 120 mW of 461 nm light, but the conversion efficiency ($\eta < 30\%$) was limited by the strong power imbalance of the two pump sources [14]. To allow a more efficient cooling of atomic strontium, a new powerful and more convenient blue source from direct second-harmonic generation (SHG) of a master-oscillator-power-amplifier (AlGaAs-MOPA) delivering an output power of 450 mW was then constructed. But unlike in the experiment in Ref. [9] that uses a critically phase-matched KNbO$_3$ semi-monolithic resonator to generate the same wavelength, we made our choice on periodically-poled potassium titanyl phosphate (PPKTP). Electric-field poled quasi-phase-matched (QPM) oxide ferroelectrics such as PPLN (periodically-poled lithium niobate) and PPKTP have recently super-seeded the previous birefringence phase-matched materials for visible light generation [15,16,17] owing to their much higher effective nonlinearities (d_{eff}(PPLN) $\sim 17-18\,\mathrm{pm/V}$ and d_{eff}(PPKTP) $\sim 7-9\,\mathrm{pm/V}$). Furthermore QPM materials are intrinsically free of walkoff. For blue generation, PPKTP is preferred to PPLN which exhibits strong photorefractive damage when used at room-temperature. In Ref. [15], an intra-cavity PPKTP frequency-doubled Nd:YAG laser yielded an output power of 500 mW at 473 nm with an internal efficiency of 5.5%. Green light power of 117 mW was generated by Juwiler *et al* from 208 mW of CW Nd:YAG laser with an efficiency of 56.5% in a semi-monolithic standing-wave

resonator, limited by strong thermal lensing effects induced by the 532 nm residual absorption [16]. In Ref. [17] a MOPA diode laser (0.5 W) similar to ours generated 200 mW of blue light at 461 nm in a ring enhancement cavity, a value comparable to that obtained using a similar semi-conductor laser, at identical wavelength, in a semi-monolithic standing-wave $KNbO_3$ resonator [9].

However due to the lower UV bandgap energy of KTP, linear absorption becomes an issue at wavelengths shorter than 500 nm. A detailed absorption measurement of flux-grown or hydrothermally-grown KTP in the spectral range from the bandgap wavelength (365 nm) to 600 nm revealed a large fluctuation from sample to sample [18]. At 473 nm for instance, values of α ranging from 0.034 to 0.085 cm^{-1} were reported. In a recent closely-related PPKTP-SHG experiment pumped at 846 nm, a value $\alpha(423 \text{ nm}) = 0.10 \text{ cm}^{-1}$ has been measured [19]. Strong thermal lensing effects [20] arising from the blue absorption was the main limitation of their power efficiency scaling in genuine CW operation ($\eta = 60\%$, corresponding to 225 mW of 423 nm power for 375mW of mode-matched Ti:sapphire laser). Higher blue power (400 mW) could be obtained for the same circulating power of $P_c = 5.5$ W only in pulsed fringe-scanning mode that allows more efficient heat dissipation within the PPKTP crystal. Such a severe limitation in CW operation actually arised from the tight focusing used ($w_0 = 17 \, \mu$m, corresponding to the theoretical optimum of the single-pass efficiency for the PPKTP crystal length $L_C = 10$ mm [22,23]) and the associated thermal lens power which scales as w_0^{-2} [20]. In true CW operation, the thermal focal length (which can be as short as a few cm, see section 6) experienced by the circulating fundamental power impedes efficient mode-and-impedance matching of the input beam. For a symmetric linear resonator for instance, thermal lensing has been shown to be responsible for the clamping of the circulating power to a low critical value P_c^{crit} corresponding to the collapse of the secondary thermally-induced waists [20].

In the present experiment, we deliberately avoid optimal single-pass focusing to circumvent these thermal lensing effects. In section 2 we show that owing to the large nonlinearity of PPKTP, one doesn't require extremely low intra-cavity linear losses to maintain the conversion efficiency constant over a wide range of focusing parameters. The latter is defined by $L = L_C/z_R$, where L_C is the PPKTP length and $z_R = k_\omega w_0^2/2$ is the Rayleigh range of the cavity mode. We find that loose focusing to $w_0 = 40 \, \mu$m in a 20 mm long PPKTP crystal still results in a large single-pass efficiency $\Gamma = P_{2\omega}/P_c^2 \sim 2.3 \times 10^{-2} \, \text{W}^{-1}$ and in a stable CW operation of the resonant cavity at the maximum available mode-matched power of $P_\omega^{\text{in}} = 310$ mW with no evidence of serious lensing effect. Using such a strategy, blue power scaling to half a Watt should be possible with ~ 0.7 W of mode-matched input power.

In section 3 we briefly describe the experimental setup, highlighting some measurement procedures aimed at an accurate determination of important

parameters such as the mode-matching factor κ or the circulating power P_c. Section 4 is devoted to the intracavity measurement of the conversion efficiency that determines the final enhancement efficiency, taking profit of the TEM_{00} resonator mode filtering of the fundamental MOPA laser non-Gaussian beam and making use of the accurate evaluation of the Gaussian beam SHG focusing function h [23]. From these measurements, we derive a consistent value of the d_{33} nonlinear tensor element of KTP. The comparison of the recorded temperature tuning curve with the functional dependence given by two of the most recently published linear and thermo-optic dispersion relations of KTP [24,25] shows a perfect agreement between theory and experiment, providing thus a stringent validation test of those dispersion relations for PPKTP in the blue/near-IR spectrum. Having determined all the relevant parameters, we then present (section 5) the resonant enhancement results which are in good agreement with the theoretical expectation, with a record efficiency of $\eta = 75\%$. The paper ends with a brief thermal effects analysis (section 6) which supports that the experiment is indeed not limited by thermal effects.

2 Analysis of singly-resonant SHG efficiency versus focusing

We start by investigating the dependence of the power conversion efficiency on the focusing parameter L. At zero cavity detuning, the internal circulating FF power P_c in a singly-resonant ring resonator is given by [3,26]

$$\frac{P_c}{P_\omega^{\text{in}}} = \frac{T_1}{\left[1 - \sqrt{(1-T_1)(1-\epsilon)(1-\Gamma P_c)}\right]^2} \tag{1}$$

where $T_1 = 1 - R_1$ is the transmission factor of the input coupler, ϵ is the distributed round-trip passive fractional loss (excluding T_1). Γ, expressed in W^{-1}, is the depletion due to non linear effects. It can be written as the sum of two terms :

$$\Gamma = \Gamma_{\text{eff}} + \Gamma_{\text{abs}} \tag{2}$$

- Γ_{eff} is the conversion efficiency, $P_{2\omega} = \Gamma_{\text{eff}} P_c^2$
- Γ_{abs} is the efficiency of the Second Harmonic absorption process, which cannot be neglected here, $P_{\text{abs}} = \Gamma_{\text{abs}} P_c^2$

The net power conversion efficiency η calculated from (1) obeys the implicit equation [7]

$$\sqrt{\eta} \left[2 - \sqrt{1-T_1}\left(2 - \epsilon - \Gamma\sqrt{\frac{\eta P_\omega^{\text{in}}}{\Gamma_{\text{eff}}}}\right)\right]^2 - 4T_1\sqrt{\Gamma_{\text{eff}} P_\omega^{\text{in}}} = 0. \tag{3}$$

4

Given Γ, which depends on the focusing and the crystal length, and given ϵ and the maximum available mode-matched P_ω^{in}, η in Eq. (1) can be optimized against T_1 to yield

$$T_1^{\text{opt}} = \frac{\epsilon}{2} + \sqrt{\left(\frac{\epsilon}{2}\right)^2 + \Gamma P_\omega^{\text{in}}} \tag{4}$$

The conversion efficiency Γ_{eff} can be evaluated using the undepleted pump SHG theory taking linear absorption into account [22,23]. For a waist location at the centre of the crystal it can be written as [23,27]

$$\Gamma_{\text{eff}} = \frac{P_{2\omega}}{P_c^2} = \frac{2\omega^2 d_{\text{eff}}^2}{\pi \epsilon_0 c^3 n_\omega^2 n_{2\omega}} L_C k_\omega \exp(-\alpha_{2\omega} L_C) \, h(a, L, \sigma) \tag{5}$$

$$h(a, L, \sigma) = \frac{1}{2L} \int_{-L/2}^{+L/2} \int d\tau d\tau' \frac{\exp[-a(\tau + \tau' + L) - i\sigma(\tau - \tau')]}{(1 + i\tau)(1 - i\tau')}. \tag{6}$$

In Eqs (5)-(6), $k_\omega = 2\pi n_\omega/\lambda_\omega$ is the FF wavevector internal to the medium, $\alpha_{n\omega}$ ($n = 1, 2$) are the linear absorption coefficients, $a = (\alpha_\omega - \alpha_{2\omega}/2)z_R$, $L = L_C/z_R$ is the focusing parameter (which differs by a factor 2 from the definition given by Boyd and Kleinman [22]) and $\sigma = \Delta k \cdot z_R$ is the normalized wavevector mismatch given by

$$\Delta k(T) = k_{2\omega}(T) - 2k_\omega(T) - 2\pi/\Lambda(T). \tag{7}$$

$\Lambda(T)$ is the PPKTP grating period whose temperature dependence can be calculated with published thermal expansion coefficients of KTP [21,28]. We can note that, when diffraction is considered, the value of Δk that optimizes the focusing function h versus σ is not nil as for a plane wave [23].

The Second Harmonic absorption efficiency Γ_{abs} is more difficult to express, except in two limits :

- for a plane wave, one can easily deduce the profile $P_{2\omega}(z, \alpha_{2\omega})$ for $0 \leq z \leq L_c$ from Eqs (5)-(6), and thus evaluate the absorbed power :

$$P_{\text{abs}} = \alpha_{2\omega} \int_0^{L_c} P_{2\omega}(z, \alpha_{2\omega}) dz \tag{8}$$

- when the beam is tightly focused, the conversion occurs only at the center of the crystal and then :

$$P_{\text{abs}} = \left(e^{\alpha_{2\omega} \frac{L_c}{2}} - 1\right) \Gamma_{\text{eff}} P_c^2 \tag{9}$$

With our crystal we measured $\alpha_{2\omega} = 0.14 \, \text{cm}^{-1}$ which leads to $\Gamma_{\text{abs}}/\Gamma_{\text{eff}} = 0.1$ (resp. 0.13) in the plane wave (resp. tight focusing) limit. Given the small
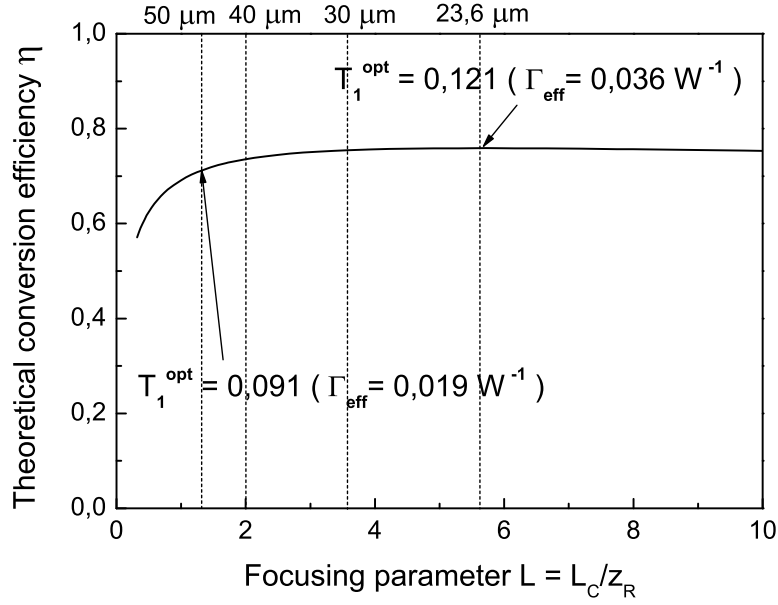
Fig. 1. Efficiency factor $\eta = P_{2\omega}/P_\omega^{\text{in}}$ versus the focusing parameter when the cavity is impedance-matched $(T_1 = T_1^{\text{opt}})$ Parameters are $P_\omega^{\text{in}} = 310\,\text{mW}$, $\epsilon = 2\%$, $d_{\text{eff}} = 9,5\,\text{pm/V}$ and $\alpha_{2\omega} = 0.14\,\text{cm}^{-1}$. Optimal focusing is for $w_0 = 23.6\,\mu\text{m}$, giving a theoretical conversion efficiency of 76%. The labelled arrows indicate the values of the single-pass conversion efficiencies as calculated from Eqs.(5)-(6).

difference between both values and since we are mainly interested in focusing below optimal, we take for the whole analysis the plane wave value[1].

The other parameters of the model are also taken from experimental measurements (see below). We have $\epsilon = 0.02$ lumping the FF crystal linear loss (absorption + AR coating) and mirror reflection loss, a crystal length of $L_C = 20\,\text{mm}$. Our measured value for the polar tensor element of KTP $d_{33} = 15\,\text{pm/V}$ is slightly smaller than [29] and yields $d_{\text{eff}} = 9,5\,\text{pm/V}$ with the refractive indices $n_\omega \equiv n_Z(922\text{nm}) = 1.8364$, $n_{2\omega} \equiv n_Z(461\text{nm}) = 1.9188$ at $T = 30°\text{C}$ [25]. The mode-matched power is $P_\omega^{\text{in}} = 310\,\text{mW}$.

Fig. 3 displays the efficiency curve $\eta(T_1^{\text{opt}}, L)$ for a beam waist range 18 μm $\leq w_0 \leq 100$ μm. It corresponds to perfect impedance matching $(T_1 = T_1^{\text{opt}}$, see Eq. (4)) for each $\Gamma(L)$. It is clearly seen that η is practically constant over the range $20\,\mu\text{m} \leq w_0 \leq 50\,\mu\text{m}$, meaning that it is not necessary to set the cavity waist at the optimal single-pass conversion as commonly believed, in spite of the two fold reduction of Γ for the loose focusing end range. At $w_0^{\text{opt}} = 23.6\,\mu\text{m}$, the circulating optimal FF power is $P_c = 2.56\,\text{W}$ (yielding $P_{2\omega} = 236\,\text{mW}$) whereas at $w_0 = 50\,\mu\text{m}$, $P_c = 3.4\,\text{W}$ ($P_{2\omega} = 220\,\text{mW}$). For

---

[1] The predictions of the model will then be slightly too optimistic for large L

these nearly identical blue power, the thermal lens power is 4 times larger at optimal focusing than at the looser focusing. Hence to avoid thermal effects, a cavity waist between $40\,\mu$m and $50\,\mu$m would be recommended ($L \leq 2$) with an expected efficiency $\eta > 70\%$.

This insensitivity of η as a function of w_0 is due to the large nonlinear efficiency which dominates round trip passive losses, even for the not so small $\epsilon = 0.02$ chosen here. Experimentally, we indeed found that nearly optimal η was measured over a large cavity waist values, the best trade-off giving tolerable thermal effects being at $w_0 = 43\,\mu$m. In the same way, the value of T_1 is not critical. Our input coupler exhibits $T_1 = 0.12\,\%$, which causes a loss smaller than 1% on the generated blue power in comparison to $T_1^{\mathrm{opt}} = 0.10\,\%$ which would optimize η for $w_0 = 43\,\mu$m (Eq (4)).

3   Experimental setup and measurement procedures

The frequency-doubling setup is sketched in Fig. 2. A conventional unidirectional ring cavity is chosen. The commercial MOPA pump laser is made of a grating-tuned extended-cavity master diode laser in the Littrow configuration, injecting a tapered semiconductor amplifier (Toptica Photonics AG). After a -70 dB Faraday isolation stage, the MOPA provides a useful single-longitudinal-mode power $P_\omega = 450\,$mW at $\lambda_\omega = 922\,$nm, with a short-term linewidth of less than 1MHz. The transverse beam shape is far from a fundamental Gaussian mode and strongly depends on the tapered amplifier injection current. A system of lenses mode-matches the input FF beam to the bow-tie ring resonator larger waist located between the 2 plane mirrors M1 and M2. The folding angle of the ring resonator is set to 11° leading to a negligible astigmatism introduced by the two off-axis curved mirrors M3 and M4 (of radius-of-curvature 100 mm). The meniscus shape of M4 (M3) do not introduce any additional divergence of the transmitted FF or SH beam. This allows an accurate measurement (to $\pm 5\%$) of the smaller waist w_0 located at the center of the PPKTP crystal from a z-scan measurement of the TEM$_{00}$ diverging FF beam leaking out from M4. The diverging beam diameter measurement is performed at different z-location by use of a rotating knife-edge commercial device, and the cavity waist is retrieved from standard Gaussian optics laws.

The pump beam is coupled in through the partial reflector M1. Mirrors M2-M3 are high-reflectors at 922nm and M4 is dichroically-coated at $\omega, 2\omega$ with $R_\omega > 99.9\%$ and $T_{2\omega} = 98\%$. Side 2 of all optics are dual-band AR-coated with $R \leq 0.5\%$. The dual-band AR-coated PPKTP crystal (Raicol Crystals Ltd) has dimension $2 \times 1 \times 20\,$mm^3, with the z-propagation direction corresponding to the X-principal axis and the 1mm thickness sides oriented along the Z-polar axis. A first-order (50%-duty-cycle) QPM periodic grating is patterned
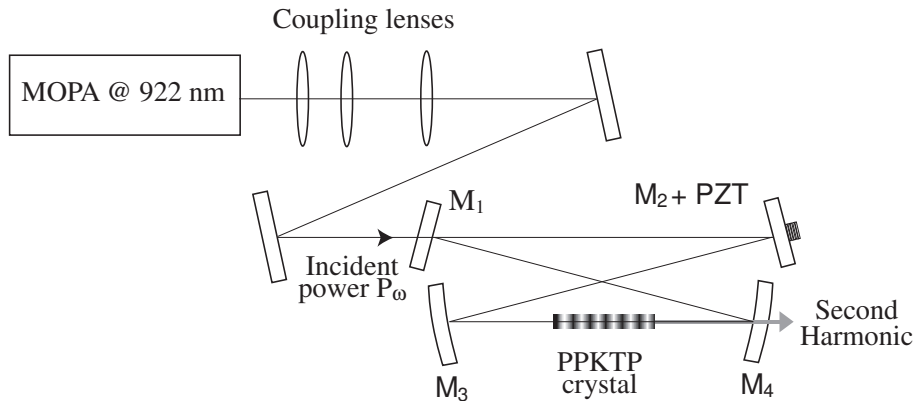
Fig. 2. Schematic of the experimental setup.

along the X-axis, with a period $\Lambda_0 \simeq 5.5\,\mu$m for temperature quasi-phase-matching around 30°C. The PPKTP chip is mounted in a small copper holder attached to a thermo-electric Peltier element with which we servo the crystal temperature to better than $\pm 10\,$mK. The crystal Z-axis is matched with the direction of the electric-field polarization of the MOPA laser. The blue absorption coefficient of this crystal $\alpha_{2\omega}$ at 461 nm was measured from a second blue source, yielding $\alpha_{2\omega} = 0.14\,(\pm 5\%)$ cm^{-1}. This value is larger than the one ($\alpha_{2\omega} = 0.10\,$cm^{-1}) measured at 423 nm by Goudarzi et al [19] on a 1cm PPKTP sample from a different manufacturer, confirming thus the large dispersion of the values from one sample to another.

Finally, because no suitable $\lambda/2$ plate was available in front of the cavity for the input power variation at constant MOPA output power, P_ω is varied with the PA injection current. As mentioned previously, such a power variation results in substantial transverse mode change and in turn in a variation of the mode-matching factor κ. The coefficient $\kappa(P_\omega)$ was hence calibrated in the absence of blue conversion (by tuning the temperature to a zero conversion regime) and used to rescale the mode-matched power. For the range $300 < P_\omega < 450\,$mW, the mode-matching factor is found practically constant and equal to $\kappa \sim 0.7$. In the following section, the conversion efficiency $\Gamma_{\rm eff}(w_0)$ (Eq. (5)) will be measured internal to the cavity. For the measurement of the circulating FF power P_c, the transmissivity of mirror M4 at 922 nm was accurately calibrated to 1.2 10$^{-5}\pm 10\%$. The FF and the SH powers were calibrated with a thermal powermeter with an uncertainty below 5 %.

4 Measurement of PPKTP effective nonlinearity and tuning curve

To model the experimental singly-resonant conversion efficiency, an accurate knowledge of the experimental $\Gamma_{\rm eff}(w_0)$ is needed. We choose not to use the standard single-pass method for the experimental measurement, since the poor
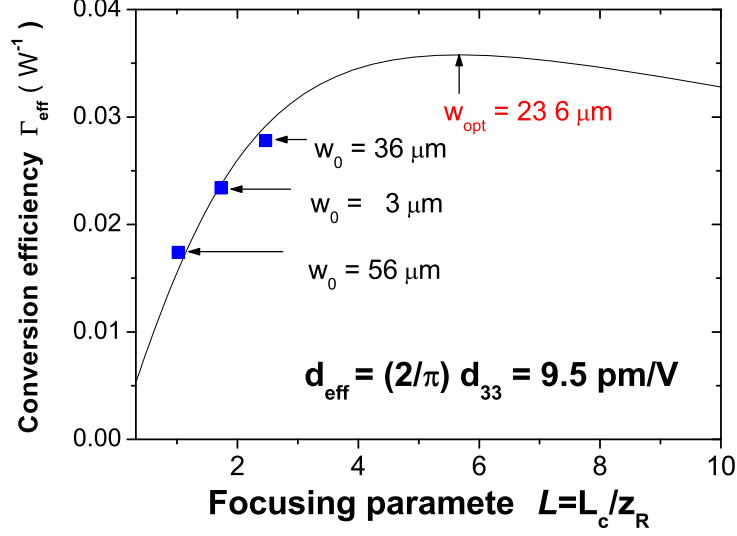
Fig. 3. Conversion efficiencies Γ_{eff} versus the focusing parameter $L = L_c/z_R$. The 3 squares are the experimental points measured at $w_0 = 56, 43, 36\,\mu$m and the solid line are the theoretical values from Eqs.(5)-(6) using the labelled value of d_{eff} after optimisation of the focusing function h over the mismatch parameter σ. The theoretical optimal waist is found at $w_{\text{opt}} = 23.6\,\mu$m.

beam quality of the MOPA output would contradict the Gaussian pump assumption of Eq.(6). By placing the PPKTP inside the resonator, the mode filtering effect of the cavity provides instead a pure TEM$_{00}$ pump beam with accurately known waists from the measurement method outlined in the previous section. Provided that pump depletion can be neglected, the intracavity power is considered as constant all along the crystal, and is defined as the solution of Eq (1).

Several values of Γ_{eff} were measured for a range of P_c and 3 waists values $w_0 = 56, 43, 36\,\mu$m, to yield respectively $\Gamma_{\text{eff}} = 0.017, 0.023, 0.028\,(\pm 10\%)\,\text{W}^{-1}$. The data points of $P_{2\omega}$ versus P_c^2 were excellently fitted by a linear function, meaning that the low depletion assumption holds for all achievable P_c's, which is confirmed by an *a posteriori* consistency check of the upper bound value $\Gamma P_c < 0.08 \ll 1$. In Fig. 3, the resulting $\Gamma_{\text{eff}}(w_0)$ are plotted against the focusing parameter L along with the theoretical curve (Eq.(5)).

The only adjusted parameter to match the experimental points to the curve is the effective nonlinear coefficient $d_{\text{eff}} = (2/\pi)d_{33}$ for a first-order QPM, which is found to be $d_{\text{eff}} = 9.5\,(\pm 5\%)\,\text{pm/V}$. Such a value is slightly higher than those measured elsewhere (5-8 pm/V) from OPO threshold measurement or difference frequency generation [24,29], even when wavelength dispersion is accounted for. This value yields for KTP $d_{33}(461nm) = 15\,(\pm 5\%)\,\text{pm/V}$, which is the commonly reported value of this polar $\chi^{(2)}$ tensor element [29,30,31] and matches exactly the value (14.8 pm/V) reported by the manufacturer [32]. This
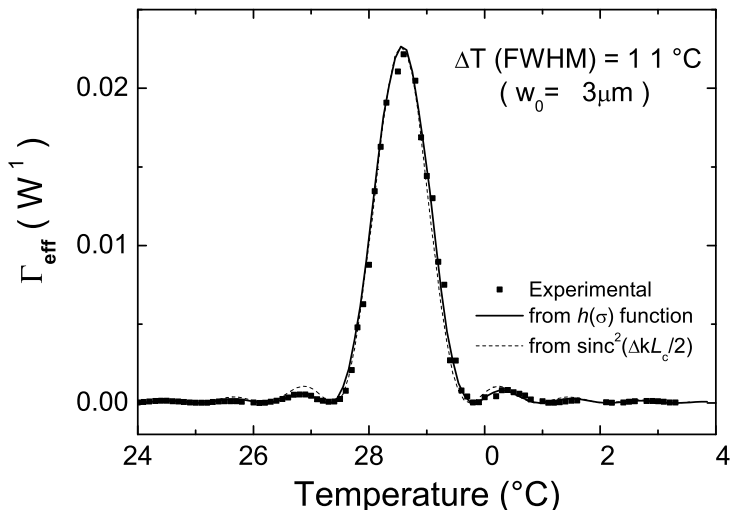
9

Fig. 4. Measured (black circles) and calculated (solid line) temperature tuning curve at $w_0 = 43\,\mu$m. The dashed line corresponds to a plane wave.

result shows that the grating quality of our cristal is extremely high. We believe that the perfect match of d_{eff} with its maximum theoretical value stems from the pure Gaussian beam measurement and analysis taking diffraction and absorption effects into account, which is not always the case with some of the reported lower values even accounting for grating periodicity defects.

We have tried tight focusing close to the optimal waist shown in Fig. 3 without any improvement in the singly-resonant conversion efficiency, despite the larger Γ_{eff}, confirming the prediction of Section 2. At $w_0 = 36\,\mu$m, the conversion efficiency is identical to the one at $43\,\mu$m. As expected, increasing thermal effects occurred with smaller waists, which could be assessed from a broadened triangular bistable shape of the FF and blue fringes as the cavity length is swept on the contracting length side of the voltage ramp (see e.g. Fig. 10 of Ref. [19] and the thermal effects analysis in Section 6). On this side of the fringe, passive self-stabilization of the optical path length of the resonator tends to maintain the cavity in resonance with the incoming FF frequency. Such an opto-thermal dynamics of thermally-loaded resonators has been analyzed in detail in Ref. [20]. Furthermore, the active locking of the cavity to the top of the distorted fringe - a bistable operating point [20] - becomes problematic as reported in Ref. [19].

The temperature tuning curve measured internal to the cavity is also shown in Fig. 4 for the final waist choice of $w_0 = 43\,\mu$m, corresponding to $L = 1.73$. The oscillatory fine structure pattern at the wings is clearly seen. The solid line is the conversion efficiency computed from Eqs.(5)-(7), where the wavevector mismatches $\Delta k(T)$ have been computed with the Sellmeier relations at room-temperature given in Ref. [24], the thermo-optic dispersion relation of

10

Ref. [25] and the thermal expansion coefficient $\alpha_X = 6.8 \times 10^{-6}/°\text{C}$ reported in Ref. [28]. Given the short grating period, a strikingly excellent agreement is seen with the data points (sidelobe amplitudes and positions) when the $h(\sigma)$ focusing function is used instead of the plane-wave formula. Apart from a lateral temperature shift of the calculated tuning curve in Fig. 4, we stress again that no fit was made to get such an agreement, which not only provides a stringent validation of the used dispersion data, at least for PPKTP produced by our manufacturer, but also highlights the excellent quality of the first-order periodic grating over the whole PPKTP length. The FWHM temperature tuning bandwidth is $\Delta T = 1.1°\text{C}$.

5 Resonant enhancement efficiency

The final cavity dimensions yielding the least thermal effects while providing the best power conversion efficiency when the cavity length is servo-controlled correspond to cavity waists $(w_0, w_1) = (43\,\mu\text{m}, 163\,\mu\text{m})$ given by a M3-M4 spacing of $\sim 130\,\text{mm}$ and a total ring cavity round-trip length $L_{\text{cav}} = 569\,\text{mm}$. For genuine CW stable operation, an active electronic servo based on an FM-to-AM fringe modulation technique was preferred to the optically phase-sensitive Hänsch-Couillaud method that was reported to fail when thermal effects arise [8,19].

The round-trip intracavity fractional loss ϵ is measured by fitting, at the QPM temperature, the total losses $p = \epsilon + \Gamma P_c$ of the cavity as a function of P_c. Otherwise, p is related to the contrast C of the cavity reflection fringes :

$$p = \frac{C\,P_\omega}{P_c} \tag{10}$$

This relationship is very reliable since it doesn't depend on the mode matching coefficient κ. The fit yields $\epsilon = 0.021\,(\pm 5\%)$, which is further checked from the value of the cavity finesse $\mathcal{F} \simeq 40$ in the absence of nonlinear conversion. This also gives a measurement of Γ which is consistent with the value quoted above.

When the cavity is close to impedance matching, the reflection contrast becomes nearly constant and is then equal to the mode matching coefficient, we measured $\kappa\,(P_\omega^{max}) = 73\,\%$. For intermediate values of the pump power, the evaluation is more difficult : κ can be deduced from the contrast of reflected fringes at zero conversion, once ϵ is known.

The generated blue power and net power efficiency η are plotted against the mode-matched power in Fig. 5 and Fig. 6. The solid lines are computed from Eq. (3) using the experimentally measured parameters. Experimental dots
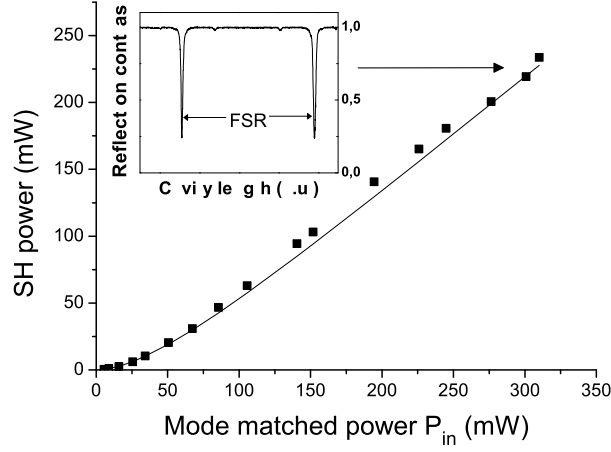
Fig. 5. SH power versus the mode-matched FF power. The solid line is a calculation from Eq. (3) making use of $\epsilon = 0.021$, $T_1 = 0.12$, $\Gamma = 0.023\,\mathrm{W}^{-1}$. The inset shows the FF reflection fringe contrast at maximum power.
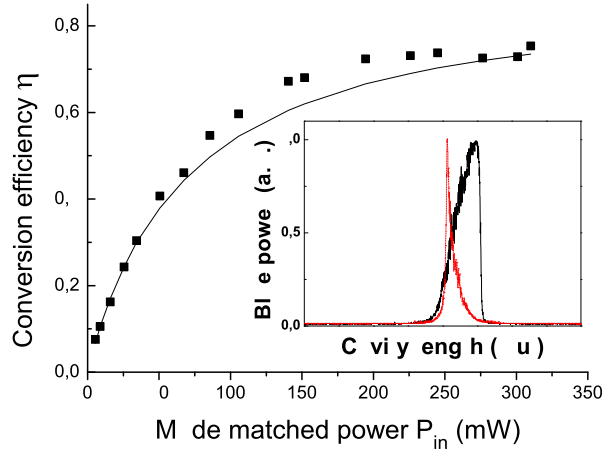

Fig. 6. SH power efficiency versus the mode-matched FF power. The solid line is again computed from Eq. (3) with the same parameter as for Fig. 5. The inset shows a magnification of the blue fringe recorded at maximum power (solid line: contracting cavity length, dotted line: expanding length). The small difference in their relative width witnesses low thermal effects as compared with Ref. [19].

match well this curve, meaning that thermal effects are not a problem up to the maximum available laser power. The small offset between experimental points and the theoretical curve from 100 mW to 250 mW being probably due to the less accurate evaluation of the mode matched power in this range. At maximum power, the finesse drops to $\mathcal{F} \simeq 30$ due to the nonlinear loss (see inset of Fig. 5 which shows the reflected FF fringe with a contrast of $\sim 73\,\%$). The conversion efficiency is independent on whether the measure-

ment is made under pulsed scanning-mode or under cavity-locked operation. In the latter case however, a slight adjustment of the PPKTP temperature has to be performed to cancel the temperature-induced phase-mismatch under CW operation (Section 6). At the maximum mode-matched input power $P_\omega^{\text{in}} = 310\,\text{mW}$ ($P_c = 3.2\,\text{W}$ is the corresponding circulating power), one obtains $P_{2\omega} = 234\,\text{mW}$ corresponding to $\eta = 75\%$.

6   Blue-induced thermal effects analysis

The inset of Fig. 6 shows a slight fringe asymmetry observed on both the FF and SH fringes, reminiscent of the onset of thermal bistability. On the contracting cavity length scan (solid line), the fringe is broadened because the opto-thermal dynamics on this side is characterized by a self-stabilizing effect of the optical path to the laser frequency whereas on the expanding length side (dotted curve) the feedback is positive [20]. In the PPKTP experiment of Ref. [19], the thermal effects were so prominent that the fringe shape broadens over several cold cavity linewidths to acquire a triangular shape. In our case, the broadening is comparatively very modest. It is expected that heating is due to both the residual FF absorption and the SH absorption. To quantify further the role of residual thermal effects, we use the radial heat diffusion model detailed in Ref. [20], assuming an equivalent crystal rod radius equal to the half-thickness of the PPKTP ($r_0 = 0.5\,\text{mm}$). The temperature rise due to the FF absorption can then be written as $\Delta T \equiv T - T_0 = \Delta T_0 - \frac{1}{2}\rho r^2$ where T_0 is the nominal phase-matching temperature in the absence of heating and r is the radial coordinate. The uniform temperature shift ΔT_0 expresses as

$$\Delta T_0 = \frac{\alpha_\omega P_c}{4\pi K_c}\left[0.57 + \ln\left(\frac{2r_0^2}{w_0^2}\right)\right] \equiv k P_c. \tag{11}$$

The quantity $\alpha_\omega P_c$ denotes the absorbed power per unit length. The quadratic term coefficient in ΔT, responsible for lensing, is $\rho = \alpha_\omega P_c/(\pi K_c w_0^2)$ with a corresponding thermal lens power

$$p = \frac{1}{f_{\text{th}}} = \frac{P_\omega^{\text{abs}}}{\pi w_0^2}\left(\frac{\mathrm{d}n_\omega/\mathrm{d}T}{K_C}\right) \tag{12}$$

where $P_\omega^{\text{abs}} = \alpha_\omega L_C P_c$ is the total FF absorbed power ($P_\omega^{\text{abs}} = 19.5\,\text{mW}$ at $P_c = 3.25\,\text{W}$ for $\alpha_\omega = 0.3\,\%\,\text{cm}^{-1}$). The quantity in parenthesis, $\zeta = \frac{\mathrm{d}n_\omega/\mathrm{d}T}{K_C}$, is the thermal figure-of-merit of KTP with $K_c = 3.3\,\text{W/(m·°C)}$ [21] and $\mathrm{d}n_\omega/\mathrm{d}T = 1.53 \times 10^{-5}$ [25]. The normalized FF fringe lineshape under adiabatic length scan $y(\delta) = P_c(\delta)/P_{cm}$, where $P_c(\delta = 0)$ is the maximum intra-

cavity power given by Eq.(1), is described by

$$y(\delta) = \frac{1}{1 + [\delta - \Delta y(\delta)]^2}.$$

(13)

where $\delta = (\nu_L - \nu_{\text{cav}})/\gamma$ is the normalized cavity detuning, γ being the cold fringe half-linewidth : $\gamma = c/[L_{\text{cav}} + L_c(n_\omega - 1)]/2\mathcal{F} = 8.5\,\text{MHz}$.

In Eq. (13), the Airy function has been approximated by a Lorentzian in the vicinity of the resonance. For $\Delta \neq 0$, the cavity resonance is seen to move adiabatically as the crystal is thermally loaded. The FWFM of the thermally broadened resonance is given in unit of γ by $\Delta = \alpha_\omega \mathcal{F} L_C P_c \zeta / 2\pi\lambda_\omega$ [20]. For a sufficiently strong thermal load ($\Delta \gg 1$) the fringe shape presents an hysteresis behavior, the saddle-node point corresponding to the top of the fringe.

For $P_c = 3.25\,\text{W}$, one finds $\Delta T_0 = 0.14°\text{C}$, and $f_{\text{th}} = 65\,\text{mm}$. Such a short focal length means that significant FF lensing still occurs despite the looser focusing used and the small value of FF absorption coefficient. Only a rigorous hot ring cavity waist analysis, similar to the one developed for a standing-wave symmetric resonator in Ref. [20], can give an indication on the influence of this thermal lens on the cold cavity waist. For a symmetric resonator, the length must be reduced to the minimum allowed space in order to contain the thermal lens effect. Due to ΔT_0, the FF hot fringe is shifted from the cold fringe position by $\Delta \simeq 0.47$ half-linewidth only, given $\mathcal{F} \sim 30$.

To evaluate the heating due to the SH absorbed power, Eq. (11)-(12) cannot be used as they are, because the blue power is not uniform along the crystal ($P_{2\omega} = 0$ at $z = 0$ and is maximum at $z = L_c$). It is however possible to estimate the total blue absorbed power $P_{2\omega}^{\text{abs}} = \Gamma_{\text{abs}} P_c^2$ from Eq. (8), which yields $P_{2\omega}^{\text{abs}} = 25\,\text{mW}$, and $\Gamma_{\text{abs}} = 2.4\,10^{-3}\,W^{-1}$. This heating power can be distributed uniformly if we define an effective absorption coefficient and an effective incoming power such that $\alpha_{2\omega} P_{2\omega} = P_{2\omega}^{\text{abs}}/L_c = 0.012\,\text{W/cm}$. Making now use of Eq. (11) with $w = w_0/\sqrt{2}$, one is lead to $\Delta T_0 = 0.34°\text{C}$. With both FF and SH heating sources, the scanning fringe lineshape becomes

$$y(\delta) = \frac{1}{1 + [\delta - \Delta y(\delta) - \Theta y^2(\delta)]^2}.$$

(14)

where $\Theta = \Gamma_{\text{abs}} \mathcal{F} P_c^2 \zeta / 2\pi\lambda_\omega \simeq 0.67$. The above fringe analysis holds as long as BLIIRA or additional photochromic phenomena, which induce further FF absorption, is neglected.

The nonlinear equation (14) is solved for y as a function of the detuning δ to model the SH fringe shape $y^2(\delta)$. Figure 7 shows the experimental blue fringe recorded for a low-rate contracting-length scan ($f = 20\,\text{Hz}$), superimposed with the calculation from Eq (14) with either $\Theta = 0$ (i.e. considering only FF heating, dotted curve) or with both FF and SH heating (solid line).
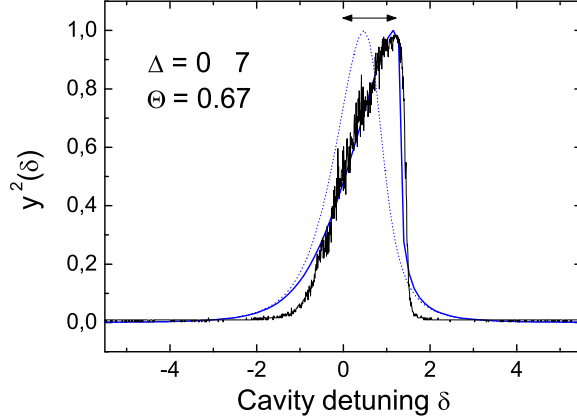
14

Fig. 7. Blue fringe shape under adiabatic cavity length scan on the negative feedback side of the triangular voltage ramp. Dotted line: FF thermal load only; solid line: FF and SH thermal load. The arrow shows the shift $\sim \Delta + \Theta$ from the cold Lorentzian centered at $\delta = 0$ (not shown).

From the analysis, the weak thermal dynamics is mainly ruled by the SH absorption. No bistability is observed meaning that these thermal effects do not affect the measured conversion efficiency, contrary to the case of Ref. [19] where the fringe shift amounts to $> 15\gamma$, giving a broad triangular shape and a sharp spike on the expanding-length scan. Indeed, considering a shorter $L_c = 1\,\mathrm{cm}$ PPKTP at near optimal focusing ($w_0 \sim 20\,\mu\mathrm{m}$), a lower value $\Gamma_{\mathrm{eff}} = 0.008\,\mathrm{W}^{-1}$ as measured in Ref. [19] for $P_\omega^{\mathrm{in}} = 360\,\mathrm{mW}$, one is lead to the same efficiency $\eta \sim 73\%$ but with a larger $P_{cm} = 5.72\,\mathrm{W}$ and $\mathcal{F} = 50$. With only twice the intracavity FF power, $\Delta T_0(\mathrm{FF}) = 0.32°\mathrm{C}$, $f_{\mathrm{th}} = 15.7\,\mathrm{mm}$ and $\Delta T_0(\mathrm{SH}) = 2.6°\mathrm{C}$.

For this tighter focusing case, the corresponding blue fringe shape plotted in Fig. 8 displays a bistable shape. On the contracting-length direction (to the right) a fringe broadening by $\Delta + \Theta = 5.8$ (in unit of γ) is evidenced. On the expanding-length direction (to the left), the opto-thermal feedback is positive. Once the upper intensity branch is reached, instead of following it back adiabatically as yielded by the stationary calculation, a sharp fringe results as sketched by the dotted line.

7   Conclusion

We have generated more than 230 mW of blue power at 461 nm starting from $P_\omega^{\mathrm{in}} = 310$ mW of mode-matched fundamental power from a MOPA diode laser, with a net power efficiency $\eta = 75\%$ using an external-cavity enhanced
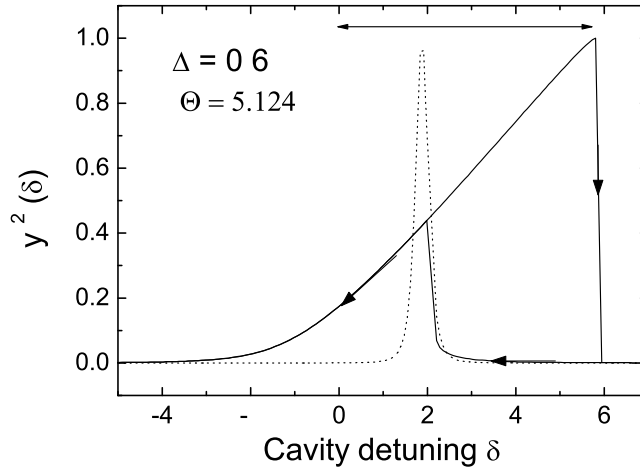
Fig. 8. Same calculation as in Fig. 7 performed here for stronger thermal effects corresponding to $P_{cm} = 5.7\,\text{W}$, with $P_{\omega}^{\text{abs}} = 17\,\text{mW}$ and $P_{2\omega}^{\text{abs}} = 128\,\text{mW}$ ($L_c = 10\,\text{mm}$, $w_0 = 20\,\mu\text{m}$). The dotted line would be the sharp fringe observed on the reverse scan direction.

PPKTP frequency doubler. The key ingredient for such a high efficiency is the use of a long crystal length allowing to relax the focusing parameter to a level where thermal effects due to the strong blue absorption (temperature mismatch and lensing effects) don't prevent from a CW operation at maximum power. No cavity locking issue for stable CW were encountered at maximum laser power. The long nonlinear interaction length results in a large single-pass conversion efficiency that relaxes the constraint of having vanishing round-trip linear loss.

Finally, by measuring the effective nonlinear coefficient internal to the ring cavity, we have additionally provided an accurate determination of the $d_{33}(461\,\text{nm}) = 15 \pm (5\%)\,\text{pm/V}$ nonlinear tensor element of KTP from exact Gaussian beam SHG theory accounting for absorption by the crystal. The high-quality of the first-order QPM grating of our sample was also checked from the perfect agreement of the measured phase-matching temperature bandwidth with a set of published Sellmeier equations and thermo-optic dispersion relations of KTP.

References

[1] S. Nakamura, G. Fasol, *The Blue Laser Diodes*, Springer Verlag, Heidelberg, 1997).

[2] R.T. White, I.T. McKinnie, S.D. Butterworth, G.W. Baxter, D.M. Warrington, P.G.R. Smith, G.W. Ross, D.C. Hanna, Appl. Phys. B **77** (2003) 547.

[3] W.J. Kozlovsky, C.D. Nabors, R.L. Byer, J. Quantum Electron. **24** (1988) 913.

[4] A. Hemmerich, D.H. McIntire, C. Zimmermann, T.W. Hänsch, Opt. Lett. **15** (1990) 372.

[5] B. Zysset, I. Biaggio, P. Günter, J. Opt. Soc. Am. B **9** (1992) 380.

[6] I. Baggio, O. Kerkoc, L.-S. Wu, P. Günter, B. Zysset, J. Opt. Soc. Am. B **9** (1992) 507.

[7] E.S. Polzik, H.J. Kimble, Opt. Lett. **16** (1991) 1400.

[8] M. Bode, I. Freitag, A. Tünnermann, H. Welling, Opt. Lett. **22** (1997) 1220.

[9] B.G. Klappauf, Y. Bidel, D. Wikowsky, T. Chanelière, R. Kaiser, *Detailed study of efficient blue laser source by second harmonic generation in a semimonolithic cavity for the cooling of strontium atoms*, Appl. Opt. **43**(2004) 2510.

[10] H. Mabuchi, E.S. Polzik, H.J. Kimble, J. Opt. Soc. Am. B **11** (1994) 2023.

[11] B. Beier, D. Woll, M. Scheidt, K.-J. Boller, R. Wallenstein, Appl. Phys. Lett. **71** (1997) 315.

[12] D. Woll, B. Beier, K.-J. Boller, R. Wallenstein, M. Hagberg, S. O'Brien, Opt. Lett. **24** (1999) 691.

[13] P. Li, D. Li, Z. Zhang, S. Zhang, Opt. Commun. **215**(2003) 159.

[14] I. Courtillot, A. Quessada, R.P. Kovacich, J.-J. Zondy, A. Landragin, A. Clairon, P. Lemonde, Opt. Lett. **28** (2003) 468.

[15] M. Pierrou, F. Laurell, H. Karlsson, T. Kellner, C. Czeranovsky, H. Huber, Opt. Lett. **24** (1999).

[16] I. Juwiler, A. Arie, Appl. Opt. **42** (2003) 7163.

[17] Ch. Schwedes, E. Peik, J. Von Zanthier, A.Y. Nevsky, H. Walter, Appl. Phys. B **76** (2003) 143.

[18] G. Hansson, H. Karlsson, S. Wang, F. Laurell, Appl. Opt. **39** (2000) 5058.

[19] F.T.-Goudarzi, E. Riis, Opt. Commun. **227** (2003) 389.

[20] A. Douillet, J.-J. Zondy, A. Yelisseyev, S. Lobanov, L. Isaenko, J. Opt. Soc. Am. B **16** (1999) 1481.

[21] J.D. Bierlein, H. Vanherzeele, J. Opt. Soc. Am. B **6** (1989) 622.

[22] G.D. Boyd, D.A. Kleinman, J. Appl. Phys. **39** (1968) 3597.

[23] J.-J. Zondy, Opt. Commun. **81** (1991) 427.

[24] K. Fradkin, A. Arie, A. Skliar, G. Rosenman, Appl. Phys. Lett. **74** (1999) 914.

[25] K. Kato, E. Tanaka, Appl. Opt. **41** (2002) 5040.

[26] A. Ashkin, G.D. Boyd, J.M. Dziedzic, IEEE J. Quantum Electron. **QE-2**(6) (1966) 109.

[27] J.-J. Zondy, D. Touahri, O. Acef, J. Opt. Soc. Am. B **14** (1997) 2481.

[28] D.K.T. Chu, J.D. Bierlein, R.G. Hunsperger, IEEE Trans. Ultrason. Ferroelec.& Freq. Control **39** (1992) 683.

[29] M. Pelz, U. Bäder, A. Borsutzky, R. Wallenstein, J. Hellström, H. Karlsson, V. Pasiskevicius, F. Laurell, Appl. Phys. B **73** (2001) 663.

[30] B. Boulanger, J.P. Fève, G. Marnier, C. Bonnin, P. Villeval, J.-J. Zondy, J. Opt. Soc. Am. B **14** (1997) 1380.

[31] I. Shoji, T. Kondo, A. Masayuki, M. Shirane, R. Ito, J. Opt. Soc. Am. B **14** (1997) 2268.

[32] A. Arie, G. Rosenman, V. Mahal, A. Skliar, M. Oron, M. Katz, D. Eger, Opt. Commun. 142 (1997) 265.